nature geoscience

Article

https://doi.org/10.1038/s41561-023-01264-6

Long-distance atmospheric transport of microplastic fibres influenced by their shapes

Received: 26 December 2022

Accepted: 3 August 2023

Published online: 25 September 2023



Check for updates

Shuolin Xiao 1, Yuanfeng Cui, Janice Brahney 2, Natalie M. Mahowald © 3 & Qi Li © 1

Recent studies have highlighted the importance of the atmosphere in the long-range transport of microplastic fibres. However, their dry deposition in the atmosphere is not fully understood, with the common spherical-shape assumption leading to significant uncertainties in predicting their travel distance and atmospheric residence time. Shapes of microplastic fibres vary greatly, which can be as long as 100 µm and as thin as 2 µm. Shapes of microplastic fibres may greatly affect their dry deposition in the atmosphere. Here we develop a theory-based settling velocity model for simulating atmospheric transport of microplastic fibres in different sizes and shapes. The model predicts a smaller aerodynamic size of microplastic fibres than that estimated by using volumetrically equivalent spherical counterparts. We find that the treatment of flat fibres as cylindrical ones, due to uncertainty in dimensions of sampled microplastic fibres, would cause overestimation of their dry deposition rate. Accounting for fibre thickness in sampled microplastic fibres leads to a mean enhancement of residence time by more than 450% compared to cylindrical ones. The results suggest a much more efficient long-range transport of flat fibres than previously thought.

The ubiquitous presence of microplastics, often defined as plastics smaller than 5 mm in size, imposes multiple threats to the sustainability of aquatic and terrestrial environments and ecosystems¹. The accumulation and transport of microplastics in water bodies have been well documented in previous studies², but increasing evidence from recent studies has highlighted the importance of the atmosphere as an equally important medium and transport pathway in the plastic cycle³⁻⁷. Their hazardous impacts could be further exacerbated as they progressively penetrate through the global environments and ecosystems via environmental transport^{4,8}. The situation could nevertheless be worsened by long-distance atmospheric transport that is weakly constrained by terrain topography, leading to the accumulation of microplastics in remote and distant locations, even in pristine wilderness^{5,9}.

To assess the potential impacts of the global plastic cycle on ecosystem health and environmental sustainability, we need to understand the entire environmental plastics cycle¹⁰, including their transport and fate in the atmospheric system, which is less extensively studied compared to the aquatic counterpart¹¹. Notably, research on the limb of the marine atmosphere is still lacking⁷. For the atmospheric limb of the plastic cycle, an understanding of the key drivers of long-distance atmospheric transport-and characteristics of microplastics that might favour such long-range effects-are crucial to assess the global environmental risks and to inform targeted management of high-risk-type microplastics (Fig. 1a,b).

In particular, aspherical microplastics such as microplastic fibres⁴ (MPFs) (Fig. 1b), which are very thin (on the order of 1 μ m, that is, O(1)) and long (100s µm)⁴, account for a substantial portion of directly discharged¹², airborne and deposited microplastics found in both the natural and built environments^{5,13}. These MPFs also have been shown to have a more adverse effect on the health of organisms compared to

School of Civil and Environmental Engineering, Cornell University, Ithaca, NY, USA. Department of Watershed Sciences, Utah State University, Logan, UT, USA. ³Department of Earth and Atmospheric Sciences, Cornell University, Ithaca, NY, USA. ⊠e-mail: ql56@cornell.edu

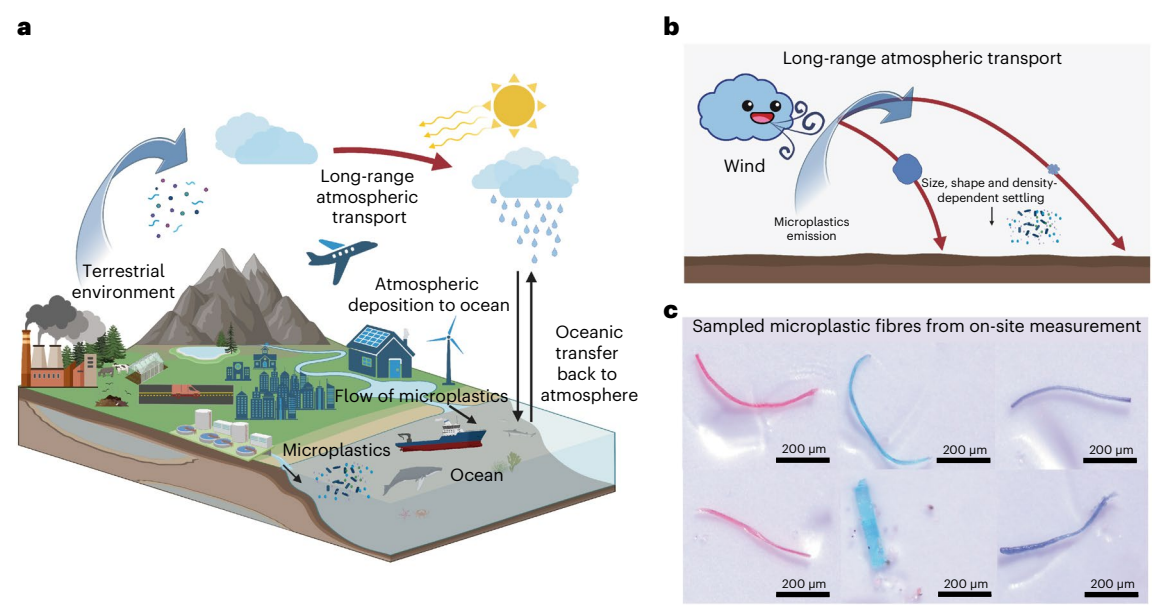


Fig. 1 | Illustrations of airborne microplastics transport fate and on-site sampled microplastic fibres with various sizes and shapes. a, Illustration of the global microplastic cycle. b, The emitted microplastics into the atmosphere undergo long-range transport and the range of transport depends on their distinct sizes, shapes and densities, which control the settling velocity.

Microplastics with smaller aerodynamic sizes can be transported to a further distance than those with larger ones. \mathbf{c} , Sampled microplastic fibres of varying cross-sectional shapes from atmospheric dry depositions ^{4,5}. Figure created with BioRender.com.

non-fibrous microplastics due to their abundance and longer retention time once consumed by biota¹⁴. However, current approaches in studying the atmospheric transport of MPFs^{3,4} adopt a spherical-shape assumption¹⁵, despite the known caveats of inaccurate prediction of the residence time of aspherical particles¹⁶. Essential to predicting the residence time, the settling velocity of MPFs in the atmosphere as a function of their size, shape and density¹⁷ still lacks a well-qualified theory. This study thus addresses a fundamental question about how the characteristics of microplastics, such as the size, aspherical shapes of MPFs and air turbulence affect their settling velocity, which is key to quantifying long-distance transport. In general, the settling velocity and the related aerodynamic size are important parameters in modelling their atmospheric transport¹³, interpreting observations of deposition amounts^{3,5} and attributing their source locations^{4,18}.

Compared to spherical particles, considerable complexity arises in predicting the settling behaviour of large-aspect-ratio MPFs^{13,19}, as their orientation and centre-of-mass settling velocity are inherently coupled^{20,21}. As shown by observations of microplastics that have undergone long-distance transport, such as in ref. 4, most of the microplastic fibre mass occurs in lengths from 50–100 µm, thus the spherical-shape assumption is expected to lead to large biases for MPFs in the atmosphere. Another critical factor contributing to the asphericity of fibres is their cross-sectional shapes; both round and flat shapes have been observed in data collected by ref. 5 (examples in Figs. 1c and 2a). Flat fibres tend to be 1–2 μ m thick and ~10–20 μ m wide, while round fibres have more similar thickness and width (-10-20 μm). Both types of fibre can be 50-300 µm long. Because the observational method is based on two-dimensional imagery, the third dimension (cross-sectional thickness) is not usually measured. Thus, due to a lack of mechanistic understanding of the effects of asphericity for atmospheric MPFs in general, the impacts of cross-sectional shapes of fibres on their settling and dry deposition lifetime (that is, residence time) are also not well understood.

Extensive studies on the settling velocity of MPFs almost exclusively focus on the aquatic environments^{22–25}. Extending these results to the air medium is not straightforward due to the contrasting density

ratios of MPFs of air versus water, for example, MPFs to air density ratio is -1,000 (ref. 2) compared to nearly neutrally buoyant MPFs in water²⁴. The non-negligible inertia of heavy aspherical particles can lead to important differences^{20,26,27} compared to nearly MPFs settling in water²⁴. Also, turbulent air motions result in complex rotational dynamics of aspherical particles^{27–31}, which may further invalidate extrapolating results obtained for fibres settling in a quiescent fluid^{22–25}. Few experimental studies on the atmospheric transport of heavy non-spherical particles exist^{32,33} to date.

It has been widely observed that MPFs undergo considerable long-range transport in the atmosphere. However, how far they reach, particularly for MPFs with varying cross-sectional shapes, remains unknown. Here we developed a method based on the slender-body theory and empirical results of heavy fibres rotation in turbulent air 21,28,29,34 to characterize the effects of MPF shapes on the settling velocity—a key parameter for predicting their atmospheric transport and fate. The newly developed model for MPFs in the atmosphere, which better agrees with available atmospheric measurements compared to previous models developed for MPFs in the aquatic environment, should be used as a basis for future models. Applying this newly developed model, we analyse factors and mechanisms that affect their settling behaviours in the atmosphere. Finally, we have quantified the effects of MPF shapes on their atmospheric dry deposition lifetime and source attributions using recently collected samples of MPFs in protected areas within US national parks⁵, providing valuable insight for future studies. Therefore, it is recommended that the newly developed model be utilized in future research related to MPFs in the atmosphere to improve the accuracy and reliability of the results.

MPF settling affected by size, shape and turbulence

We first compare the settling velocity, w_s , calculated from the newly developed semi-analytical model with counterparts derived from existing models^{22–25} and experimental data of nylon fibres settling in air³². On the basis of the measurements³², the nylon fibre's diameter and density are $47 \, \mu m$ and $1.140 \, kg \, m^{-3}$, respectively. All other models shown

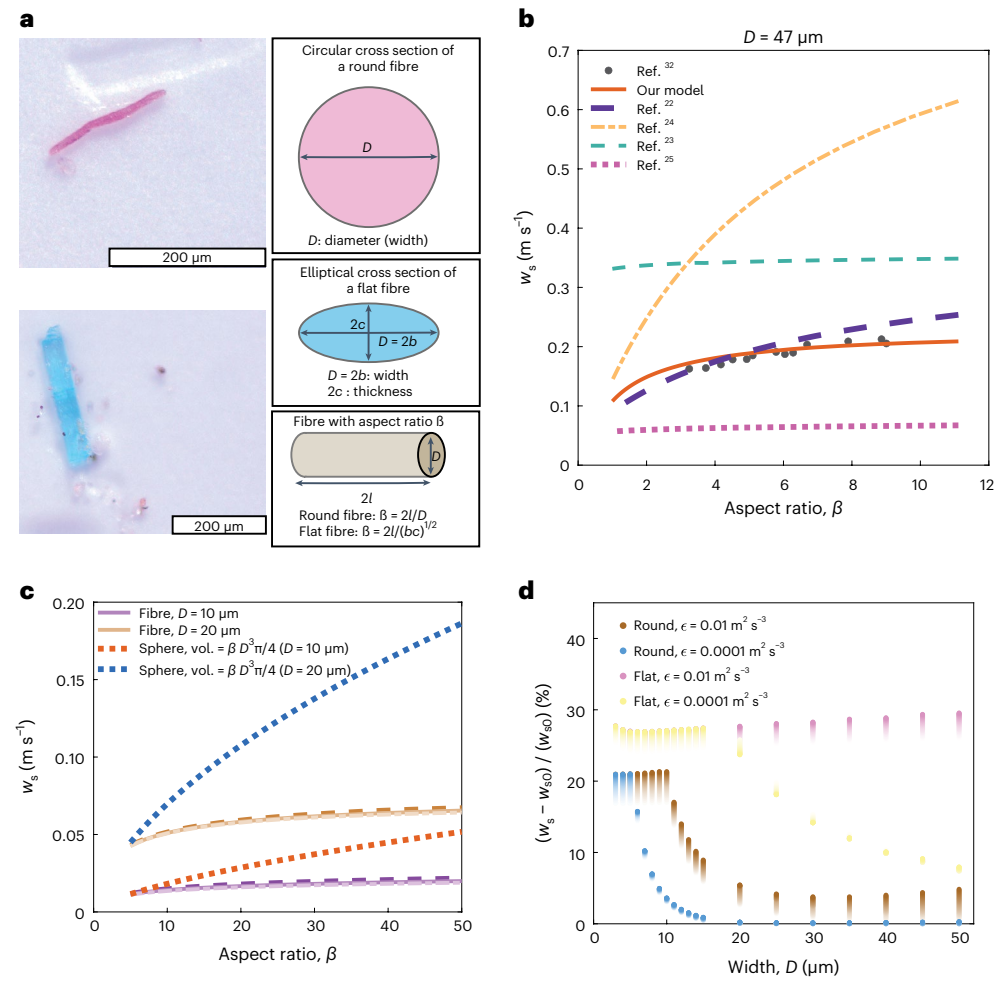


Fig. 2 | **Impacts of predictive models, geometric configurations and ambient turbulence on the settling velocity of microplastic fibres. a**, Images of observed fibres with round and flat cross sections. The half length of a fibre is *l*. The width of a circular cross section of a round fibre is its diameter, *D*. The cross section of a flat fibre can be modelled as an ellipse, where the major diameter is the width D = 2b and the minor diameter is the thickness 2c, for b and c being the semi-major axis and semi-minor axis, respectively. β is the aspect ratio of a fibre. **b**, Comparison of the settling velocities, w_s , for round fibre calculated by using the expressions proposed in this study and other existing models²²⁻²⁵ and

measurements³². **c**, The settling velocity w_s of round fibre as a function of aspect ratio β computed using the proposed model. Two diameters, D=10 and $20~\mu m$, and local turbulent dissipation rate, $\epsilon=0.0001,0.001,0.01~\text{m}^2~\text{s}^{-3}$ in dot—dash, solid and dash lines with darker coloured lines, are considered. The dotted lines show w_s for spherical particles with equivalent volumes using the Stokes drag model. **d**, The relative terminal settling velocity difference $\frac{w_8-w_{s0}}{w_{s0}}$ between MPF immersed in a flow with turbulent dissipation rate ϵ and the one surrounded by a quiescent flow as a function of the width of MPF. Increasingly darker shades of the markers indicate fibres of larger aspect ratio, where $5 \le \beta \le 50$.

in Fig. 2b have been validated for fibre settling in quiescent aquatic environment $^{22-25}$. The turbulent dissipation rate ϵ , that is, an input to our model to quantify the turbulent effect, is selected as 0.001 m² s⁻³, which is in the typical range as measured in the atmospheric boundary layer³⁵. Figure 2b demonstrates that our newly proposed model agrees well with the experimental data in ref. 32. A similar prediction is also achieved by Dietrich's model²², which is one of the most widely used semi-empirical models requiring multiple parameters as inputs. One potential caveat is that no experimental data for flat fibres settling in the air are available, to the best of the authors' knowledge. However, we expect the current model to be applicable for both round and flat fibres because the entire framework derived here is based on slender-body theory³⁶, that is, applicable for a general elongated particle with an elliptical cross section (more details shown in equations (6) and (7) in Supplementary Information and the notes therein). Future experimental results with variable cross-sectional shapes of the fibres will be useful to further verify the model.

It is revealed that w_s is determined by ambient flow condition, and its inherent properties including density, size and shape^{22,37}. We set

fibre mass density ρ_p = 1,000 kg m⁻³ for analysis. Its size and shape are uniquely specified by its width D and aspect ratio $\beta = 2l/D$ (fibre with a round cross-sectional shape or 'round fibre') or $\beta = l/\sqrt{bc}$ (fibre with a flat/elliptical cross-sectional shape or 'flat fibre') (Fig. 2a). Sensitivity analyses of the definition of the aspect ratio of flat fibre are shown in Extended Data Figs. 1 and 2. Figure 2c first compares w_s of round fibres with $D = 10 \mu m$ and 20 μm with spherical particles of equivalent volume given by $\frac{\pi}{2}\beta D^3$. The diameter D for round fibre 4,17 and turbulent dissipation rate ϵ (ref. 35) selected in Fig. 2c are within the ranges detected in the atmosphere. Figure 2c shows that D is the key determinant for w_s of fibres. Besides, β only affects w_s notably when β is small. These can be seen from equation (1) and Supplementary Note 1 that w_s has a leading-order dependence on cross-sectional area $A_f = \pi D^2 / 4$ and $\ln(\beta)$. The logarithmic dependence on β serves as a correction for the finite length effect on the drag force³⁴. In contrast, the Stokes settling velocity^{15,38} for a spherical particle of equivalent volume in quiescent fluid with diameter $D_{\text{vol}} = D(3\beta)^{1/3}$ scales with $A_f \beta^{2/3}$. The 2/3 power-law dependence instead of a logarithmic dependence on β makes the predicted magnitude of w_s much larger for spherical particles with

equivalent volumes compared to round fibres. In other words, for a given volume, the elongated shape of MPFs contributes to a marked reduction of w_s compared to a spherical-shaped particle. The effect of turbulence on round fibres is negligible for round fibres with these two diameters, and the negligible turbulence effect holds for the range of β considered here.

The ambient turbulence will affect the w_s of MPFs by altering the statistical distributions of fibre orientations as they settle due to the irregularity and randomness of turbulent air motions. We selected the aspect ratio β ranging from 5 to 50 according to data from ref. 5, and two representative turbulent dissipation rates $\epsilon = 0.01$ and 0.0001 m² s⁻³ are selected. Figure 2d demonstrates the relative difference of settling velocity w_s between MPF in turbulent flow and the one in quiescent flow with settling velocity w_{s0} . For fibres of a given width, symbols of darker colours indicate an increasing aspect ratio from 5 to 50. For round fibres with diameter $D \le 10 \,\mu\text{m}$ and $\epsilon = 0.01 \,\text{m}^2 \,\text{s}^{-3}$, the turbulence effect dominates and tends to randomize the distribution of fibre orientation measured by the azimuthal angle θ , resulting in orientation variance $\langle \cos^2 \theta \rangle$ being 1/3 and $\frac{w_s - w_{s0}}{w_{s0}}$ (expressed as $(M_{\parallel} - M_{\perp})/M_{\perp} \langle \cos^2 \theta \rangle$; Methods) approaching 20% approximately. This randomization of fibre orientation is suppressed for round fibres with larger diameters, and the fluid inertial torque becomes important, which explains the insignificant effect of turbulence seen in Fig. 2c. For a flat fibre with a width 2b up to 50 μ m and ϵ = 0.01 m² s⁻³, it always exhibits randomized

motion. Flat fibres have higher values in $\frac{w_s - w_{s0}}{w_{s0}}$ compared with round

fibres, which is due to greater variations of the area projected in the direction of gravitational force (namely larger magnitude of M_\parallel/M_\perp ; Methods). When the turbulence dissipation rate is small with $\epsilon=0.0001\,\mathrm{m^2\,s^{-3}}$, the turbulent effect on round fibre with diameter $D\ge 10~\mu\mathrm{m}$ is practically negligible, but flat fibres exhibit randomized orientations up to width $2b>20~\mu\mathrm{m}$. Beyond the randomized regime,

where $S_f \ll 1$ (Methods), $\frac{w_s - w_{s0}}{w_{s0}}$ remains non-negligible compared to

round fibres for the range of parameters considered in this study. The preference for the randomization of flat fibres by turbulence can also be explained by their rotational dynamics. The settling velocity of MPFs is the result of the balance between its net weight and the drag it experiences, which is primarily determined by the cross-sectional area. This makes flat fibres typically have a lower settling velocity than round fibres. Therefore, they experience less fluid inertia and rotational drag torques (Methods) due to their smaller $w_{\rm s}$ (ref. 28). As a result, the torque exerted by ambient turbulence plays a larger role, leading to more randomized rotational dynamics for flat fibres.

Furthermore, variation in the fibre aspect ratio at a given width and surrounding turbulent dissipation rate leads to a minor change of $\frac{w_s - w_{s0}}{w_{s0}}$

within 10% for both round and flat fibres. Noticeably, when the rotation of microplastic fibres is randomized by turbulence, a larger aspect ratio will introduce higher drag variation, making the relative magnitude

difference of the mobility matrix and thus $\frac{w_{\rm s}-w_{\rm s0}}{w_{\rm s0}}$ larger. Beyond the

randomized regime, the fibre with a larger aspect ratio will move along with the fluid and thus have higher inertia to suppress the randomness motion exerted by the turbulent ambient air, resulting in a smaller variance of fibre orientations $\langle\cos^2\theta\rangle$, which can compensate for the effect of higher drag variation. In short, the turbulent effect should be included for all the flat fibres considered here and is insignificant for round fibres with a large width, which provides a foundation to simplify the formulation of w_s as included in Supplementary Note 2.

Characterizations for on-site sampled MPFs

We then apply the newly proposed model to compute the settling velocity $w_{\rm s}$ for MPFs from atmospheric observations. The observations were obtained from samples collected from three sites in Brahney et al. ⁴

during the dry deposition process. A total of 1,260 measurements of fibre length and width were taken along with the characterization of whether the fibre was round or flat. Figure 3a shows that most MPFs have a width within 5–30 µm with $\beta \le 20$. The majority of w_s for these MPFs is of O(1) cm s⁻¹, as indicated in Fig. 3b. The variation of w_s is more sensitive to the width compared to the aspect ratio as explained in the previous section. Note that current analytical measurements cannot precisely detect the geometrical dimensions of the MPFs below -4 µm (ref. 13). Therefore, it is not easy to distinguish the exact cross-sectional shape of MPFs when their smallest dimension sizes are below the detection limit. Sensitivity of the aerodynamic sizes of sampled fibres to thickness is shown in Extended Data Fig. 3. This could lead to a substantial overestimation of the w_s if we assume the flat fibre possesses a round cross section due to the dominant dependence of w_s on $A_f \log(\beta)$ as demonstrated in the previous section.

To understand the effects of inaccurate designation of the cross-sectional shapes, we compute the geometric or aerodynamic diameter³⁹ of MPFs, which is defined here as the equivalent diameter $D_{\rm F}$ (µm) of a spherical particle that will undergo dry deposition at the settling velocity according to ref. 15. A smaller D_E signifies a smaller dry deposition rate and vice versa. First, the settling-rate equivalent geometric diameter D_{settling} is determined, which is D_{E} of a spherical particle that would have a settling velocity w_s as a fibre with either round or flat cross-sectional shapes. We also consider the geometric diameter of a spherical particle with equivalent volume as a round or flat fibre, denoted as D_{vol} . The cross-sectional equivalent D_{area} is defined as the diameter corresponding to a spherical particle that has the same projected cross-sectional area as a round or flat fibre. Figure 3c shows the distributions of $D_{\rm E}$ based on these three different definitions for all samples with measured lengths and widths. A uniform thickness of 2 μm for all flat fibres is assumed following the previous study⁴ using the same samples of MPFs. Incorrect designation of the cross-sectional shape as round instead of flat substantially overestimates the mean and the spread of D_{settling} , which highlights the importance of improving the characterization of the third and minimum dimension of the MPFs in future studies. Also, as explained in the previous section about distinct functional dependence on aspect ratio in elongated fibre compared to spherical particle, D_{vol} is larger than the one based on the settling-rate equivalent, D_{settling} . Besides, D_{area} is the smallest geometric diameter among the three because it neglects contribution to the drag due to its elongated shape. Overall, clear distinctions in terms of the mean and spread of the geometric diameters can be seen between D_{settling} , D_{vol} and D_{area} , which implies that depending on assumptions of shapes and settling velocity models used, differences in aerodynamic sizes can further impact estimates of the dry deposition lifetime for MPFs in the atmosphere.

Reduction in the dry deposition rate and enhancement of dry deposition lifetime 16 are now considered. We quantify the difference between $w_{\rm s}$ from our model and the one resulting from either incorrect modelling based on $D_{\rm vol}$ or negligence of its minimum dimension size (that is, inaccurate designation of flat fibres). Quantitatively, the reduction in dry deposition rate and enhancement of dry deposition lifetime

are defined as $1-\frac{w_{\rm s}}{w_{\rm s,equ}}$ and $\frac{w_{\rm s,equ}}{w_{\rm s}}-1$ (ref. 16), respectively, where $w_{\rm s,equ}$

is the settling velocity of a spherical particle with $D_{\rm vol}$ computed using the spherical particle model¹⁵. The cumulative distributions of the enhancement of dry deposition lifetime $\frac{w_{\rm s,equ}}{w_{\rm s}} - 1$ for MPFs measured on site, assuming either flat or round cross-sectional shapes are shown in Fig. 3d,e. The enhancement of dry deposition lifetime is about 80% if we adopt the newly proposed model instead of the one based on $D_{\rm vol}$ for MPF, with a reduction of the mean dry deposition rate of about 40% (Extended Data Fig. 4). More importantly, if we inaccurately identify flat fibres as round ones due to the difficulty in identifying the minimum dimension size, it can result in a substantial discrepancy. The mean enhancement of dry deposition lifetime is above 450%, and a mean

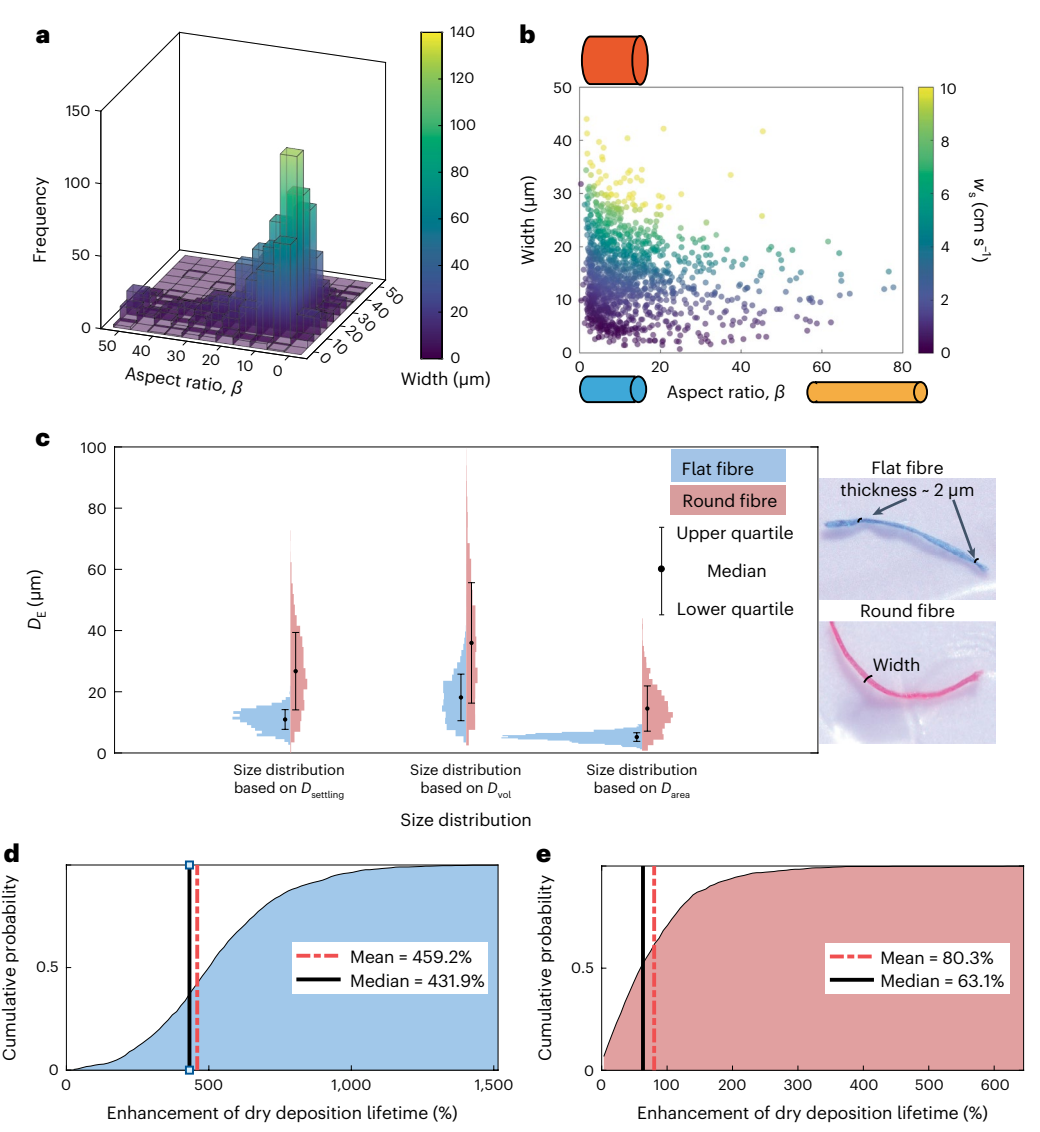


Fig. 3 | Geometric configuration, settling velocity, aerodynamic size distributions and enhanced dry deposition lifetimes of collected microplastic fibres. a, Two-dimensional histograms showing the distribution of the width and aspect ratio of the collected MPFs from field measurement. b, Terminal velocity distribution for sampled MPFs, assuming the cross-sectional shape is round. c, Violin plot for the distribution of equivalent particle size $D_{\rm E}$ (µm) based on dry deposition-rate equivalent ($D_{\rm settling}$), volumetric equivalent ($D_{\rm vol}$) and cross-section-area equivalent ($D_{\rm area}$), assuming MPFs having round

and flat cross-sectional shapes. The black dot represents the mean $D_{\rm E}$, while the whiskers indicate the range between the lower and upper quartiles for all the samples with sample size 1,260. **d**, Cumulative probability distributions of the enhancement of dry deposition lifetime assuming MPFs having a flat cross-sectional shape. **e**, Same as **d** but assuming MPFs having a round cross-sectional shape. For **d** and **e**, the red dash–dot lines denote the mean quantities, and the black solid lines represent the median values.

reduction in dry deposition rate is roughly 80% (Extended Data Fig. 4). This considerable enhancement of the dry deposition lifetime of MPF with a flat cross-sectional shape will greatly affect our estimation of the transport fate and path of the microplastic collected on site using the climate model⁴.

Effects of shape on deduced sources of MPFs

Here we explore the implications of the aforementioned new deposition velocities on our understanding of atmospheric MPFs transport. As described in more detail in ref. 4, the optimal estimation study simulates five postulated sources of microplastics: road/tyre braking 40, entrainment of ocean microplastics 41, agricultural dust, population sources and dust sources downwind of population centres. In this study, the particle sizes are forced to match the observations when normalized so that the equivalent volumetric diameter for a sphere gives the same dry deposition rates as deduced for the size and shapes from

ref. 4, assuming flat and round fibres (Methods). Figure 4a shows how these distributions vary from those using the standard dry deposition spherical equivalent models. Notice that the round cross-sectional shape assumption is equivalent to a much faster deposition velocity (larger size) compared to the flat shape assumption. Particle sizes ranging from small, medium and big are performed for sensitivity tests as described in ref. 4, and both the medium and big size tests lead to a more uniform distribution of particle sizes compared to results using the newly developed model here.

Changes in the assumptions about deposition lead to fibres that travel much less far for cylindrical versus flat fibres, which causes a shift in which sources are most likely according to the optimal estimation in Fig. 4b,c. For flat fibres, the contribution of the tyres/braking source for the mid-point value goes down compared to the previous estimates, while the ocean source contribution increases (Fig. 4b). Additional sensitivity analyses on how ocean source depends on

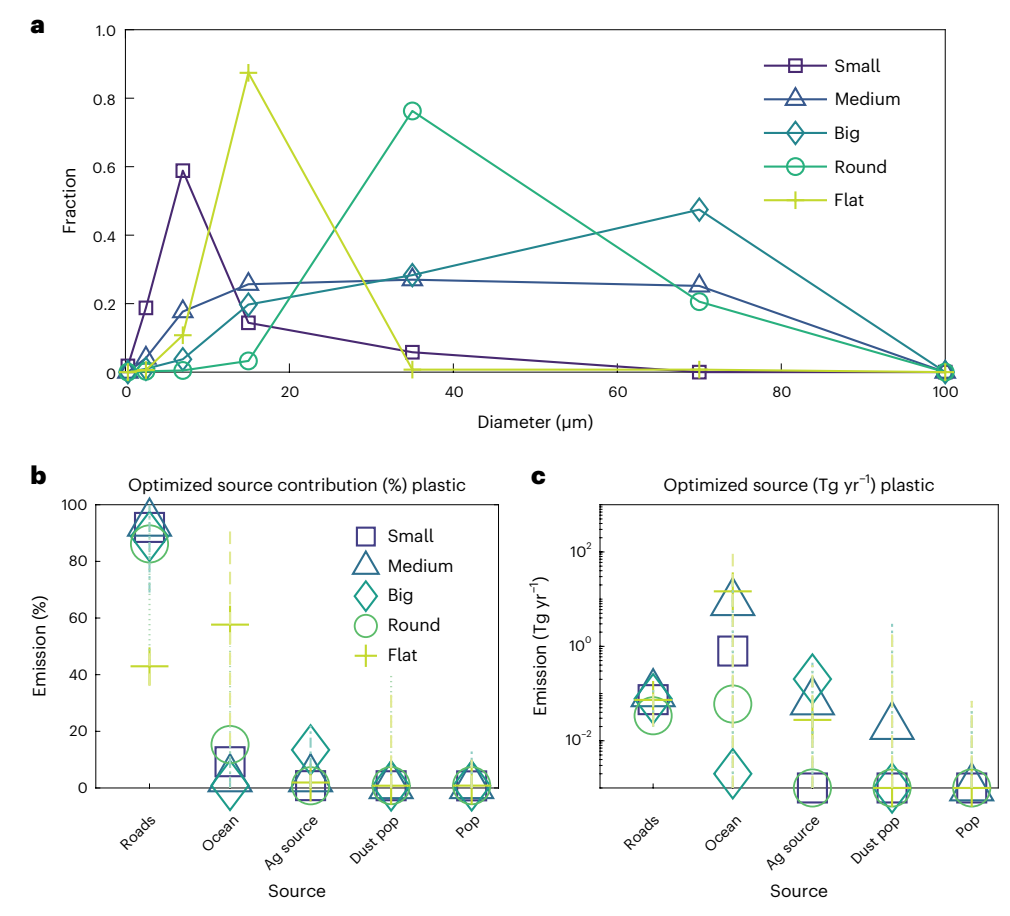


Fig. 4 | Comparative analysis of mass fractions, source contributions and global total emissions for microplastics with varied shapes and sizes.

a, Fraction of the mass in each size at deposition used in the optimal estimation for the plastics from ref. **4** (small, medium, big), compared to the 'flat' fibre and 'round' fibre dry deposition velocities used here. For 'flat' fibre and 'round' fibres, the diameter is based on D_{settling} , **b.c**, The optimal estimation of the percent contribution of different sources to the deposition at the observational sites

(b) and global total emissions for the original cases from ref. 4 (small, medium, big) and the new flat and round fibre cases developed here (c). The 95% confidence intervals for estimates based on different assumptions of shapes (that is, spheres, 'round' fibre and 'flat' fibres) are shown by dot–dash, dotted and dash lines, respectively. 'Ag source' refers to source from agricultural dust; 'Dust pop' refers to dust sources downwind of population centres; 'Pop' refers to population sources.

particle size can be found in Extended Data Fig. 5. Nevertheless, more work needs to be done regarding how microplastics from the ocean become airborne ^{41,42}. Similarly, the absolute magnitude of the deduced global source decreases for the tyres/braking source and increases for the ocean source. Notice that because the uncertainties are large in these estimates, only small shifts in the 95% are seen. However, it can still be concluded that emission source estimates are sensitive to how the setting velocity is modelled and to assumptions about their cross-sectional shapes.

Implications for atmospheric long-range transport

This study demonstrates the shape effect of MPFs on their long-range atmospheric transport. An important accomplishment of our study is the development of a semi-analytical formulation (Methods) to calculate the gravitational settling velocity of the MPFs. This formulation is based on slender-body theory and takes into account the orientation statistics of the MPFs, as parameterized by previously published numerical experimental results²⁸. In particular, the dry deposition process and related source of MPFs are strongly related to their settling velocity, which depends on their elongation, cross-sectional shapes, ambient turbulent environment and orientation, which, in turn, is determined by these three factors. The newly developed model for atmospheric MPFs can help in accurately characterizing the long-range transport

of microplastics in the atmosphere. This includes determining the lifetime of these particles in the atmosphere, the distances they can travel and the implications of the ocean being a more dominant source.

The results demonstrate that due to the elongated shape of MPFs, they have lower aerodynamic diameters compared to spherical particles of identical volume for samples from on-site measurements. This also implies that the spherical particle model for settling velocity that considers a volume-equivalent aerodynamic diameter can lead to considerable errors in terms of the dry deposition rate and lifetime in the atmosphere. As a result, source attribution based on the newly proposed gravitational settling velocity of observed MPFs suggests that the ocean might be a major contributor, especially if the fibres are of flat cross-sectional shape.

Impact of cross-section shapes of MPFs

A highlight of our formulation is that the round and flat cross-sectional shapes of MPFs are explicitly considered. The cross-sectional shape has been demonstrated as a key factor governing the settling velocity for MPFs with identical widths but different thicknesses, namely, 'round' fibre (that is, cylindrical shape) and 'flat' fibre. The theoretical underpinning of the effect of cross-sectional shape also implies that measurement of the dimension of cross-section areas of MPFs is crucial, yet it is currently overlooked. Overall, emission source estimates are sensitive to models of gravitational settling velocity and cross-sectional

shapes, further underscoring the importance of characterizing the detailed shapes and dimensions of MPFs in future atmospheric microplastic studies.

Also, our formulation indicates that the effect of atmospheric turbulence on w_s of flat fibres is more notable compared to that for round fibres, as explained in Results. A simplified model for w_s for round fibres ($D > 15 \, \mu m$) is therefore proposed here (Supplementary Information) and can be incorporated into regional and global atmospheric transport models to further investigate the atmospheric limb of the global plastic cycle. The implementation of our newly proposed model for large-scale modelling is expected to be straightforward, as evidenced by the flowchart presented in Extended Data Fig. 6.

In conclusion, the cross-sectional shape and densities play a leading-order effect in determining the long-range transport fate of MPFs, while the lengths play a secondary role. Our model can also be applied to other particles with fibrous shapes, making it suitable for extending our current work to nanoplastics, dust and tyre particles with elongated forms 43 . In our study, we only consider MPFs with a density of $1\,\mathrm{g}\,\mathrm{cm}^{-3}$; extending the model to MPFs with different densities should be straightforward.

Limitations of the study

There are certain limitations to our current work, mainly due to the assumptions and constraints inherent in our use of slender-body theory in formulation of the settling rate. Specifically, our model does not take into account the particle inertia of MPFs as characterized by $Re_D = (w_{fi} w_{fi})^{1/2} D/ve_D$ which means that it may not be directly applicable to fibres whose Re_D > 0.5 and effective width $2\sqrt{bc}$ > 50 µm. Besides, for the validity of the slender-body assumption, the aspect ratio should have $\beta = l/\sqrt{bc} > 5$, and a corrective factor has been introduced for fibres with small β by Kramel²⁸. As seen in Fig. 3a,b, most MPFs fall into the range mentioned above, and a correction has been added for fibres with small β . Notably, our model does not impose any restrictions on the shape of the fibre's cross section, making it applicable to fibres with irregular cross sections³⁶. For MPFs with much larger Re_D and effective width, detailed particle-tracking laboratory experiments and particle-resolved numerical simulations are necessary to understand the settling rate and rotational dynamics⁴⁴. Furthermore, while our study focuses on the behaviour of rigid microplastic fibres in atmospheric turbulence, we acknowledge that deformation can also nontrivially influence fibre behaviour. Future research could investigate the impact of fibre deformation on orientation, interaction with ambient turbulence and experienced aerodynamic drag. These factors can ultimately affect fibre transport and deposition patterns in the atmospheric environment.

Online content

Any methods, additional references, Nature Portfolio reporting summaries, source data, extended data, supplementary information, acknowledgements, peer review information; details of author contributions and competing interests; and statements of data and code availability are available at https://doi.org/10.1038/s41561-023-01264-6.

References

- Yang, L., Zhang, Y., Kang, S., Wang, Z. & Wu, C. Microplastics in soil: Aa review on methods, occurrence, sources, and potential risk. Sci. Total Environ. 780, 146546 (2021).
- Horton, A. A. & Dixon, S. J. Microplastics: an introduction to environmental transport processes. Wiley Interdiscip. Rev. Water 5, e1268 (2018).
- Allen, S. et al. Atmospheric transport and deposition of microplastics in a remote mountain catchment. *Nat. Geosci.* 12, 339–344 (2019).
- 4. Brahney, J. et al. Constraining the atmospheric limb of the plastic cycle. *Proc. Natl Acad. Sci. USA* **118**, e2020719118 (2021).

- Brahney, J., Hallerud, M., Heim, E., Hahnenberger, M. & Sukumaran, S. Plastic rain in protected areas of the United States. Science 368, 1257–1260 (2020).
- Abbasi, S., Rezaei, M., Ahmadi, F. & Turner, A. Atmospheric transport of microplastics during a dust storm. *Chemosphere* 292, 133456 (2022).
- Allen, D. et al. Microplastics and nanoplastics in the marineatmosphere environment. Nat. Rev. Earth Environ. 3, 393–405 (2022).
- 8. Rillig, M. C. & Lehmann, A. Microplastic in terrestrial ecosystems. *Science* **368**. 1430–1431 (2020).
- Allen, S. et al. Evidence of free tropospheric and long-range transport of microplastic at Pic du Midi observatory. *Nat. Commun.* 12, 7242 (2021).
- Thomas, K. V. Understanding the plastics cycle to minimize exposure. Nat. Sustain. 5, 282–284 (2022).
- Zhang, Y., Gao, T., Kang, S. & Sillanpää, M. Importance of atmospheric transport for microplastics deposited in remote areas. *Environ. Pollut.* 254, 112953 (2019).
- Woodward, J., Li, J., Rothwell, J. & Hurley, R. Acute riverine microplastic contamination due to avoidable releases of untreated wastewater. *Nat. Sustain.* 4, 793–802 (2021).
- 13. Zhang, Y. et al. Atmospheric microplastics: a review on current status and perspectives. *Earth Sci. Rev.* **203**, 103118 (2020).
- Taylor, M., Gwinnett, C., Robinson, L. F. & Woodall, L. C. Plastic microfibre ingestion by deep-sea organisms. Sci. Rep. 6, 33997 (2016)
- Zender, C. S., Bian, H. & Newman, D. Mineral dust entrainment and deposition (dead) model: description and 1990s dust climatology. J. Geophys. Res. Atmos. https://doi.org/10.1029/2002JD002775 (2003).
- Huang, Y. et al. Climate models and remote sensing retrievals neglect substantial desert dust asphericity. *Geophys. Res. Lett.* 47, e2019GL086592 (2020).
- 17. Kooi, M. & Koelmans, A. A. Simplifying microplastic via continuous probability distributions for size, shape, and density. *Environ. Sci. Technol. Lett.* **6**, 551–557 (2019).
- Evangeliou, N., Tichý, O., Eckhardt, S., Zwaaftink, C. G. & Brahney, J. Sources and fate of atmospheric microplastics revealed from inverse and dispersion modelling: from global emissions to deposition. J. Hazard. Mater. 432, 128585 (2022).
- Huang, Y., Qing, X., Wang, W., Han, G. & Wang, J. Mini-review on current studies of airborne microplastics: analytical methods, occurrence, sources, fate and potential risk to human beings. TrAC Trends Anal. Chem. 125, 115821 (2020).
- Marchioli, C., Fantoni, M. & Soldati, A. Orientation, distribution, and deposition of elongated, inertial fibers in turbulent channel flow. *Phys. Fluids* 22, 033301 (2010).
- 21. Lopez, D. & Guazzelli, E. Inertial effects on fibers settling in a vortical flow. *Phys. Rev. Fluids* **2**, 024306 (2017).
- Dietrich, W. E. Settling velocity of natural particles. Water Resour. Res. 18, 1615–1626 (1982).
- Khatmullina, L. & Isachenko, I. Settling velocity of microplastic particles of regular shapes. Mar. Pollut. Bull. 114, 871–880 (2017).
- Waldschlager, K. & Schuttrumpf, H. Effects of particle properties on the settling and rise velocities of microplastics in freshwater under laboratory conditions. *Environ. Sci. Technol.* 53, 1958–1966 (2019).
- 25. Zhang, J. & Choi, C. E. Improved settling velocity for microplastic fibers: a new shape-dependent drag model. *Environ. Sci. Technol.* **56**, 962–973 (2021).
- Zhao, L., Challabotla, N. R., Andersson, H. I. & Variano, E. A. Rotation of nonspherical particles in turbulent channel flow. *Phys. Rev. Lett.* 115, 244501 (2015).

- Voth, G. A. & Soldati, A. Anisotropic particles in turbulence. Ann. Rev. Fluid Mech. 49. 249–276 (2017).
- 28. Kramel, S. Non-spherical Particle Dynamics in Turbulence. PhD thesis, Wesleyan Univ. (2018).
- 29. Menon, U. K. Theory and Simulation for the Orientation of High Aspect Ratio Particles Settling in Homogeneous Isotropic Turbulence. PhD thesis, Cornell Univ. (2009).
- Marchioli, C., Zhao, L. & Andersson, H. On the relative rotational motion between rigid fibers and fluid in turbulent channel flow. *Phys. Fluids* 28, 013301 (2016).
- Zhao, L., Marchioli, C. & Andersson, H. I. Slip velocity of rigid fibers in turbulent channel flow. *Phys. Fluids* 26, 063302 (2014).
- Jayaweera, K. & Cottis, R. Fall velocities of plate-like and columnar ice crystals. Q. J. R. Meteorolog. Soc. 95, 703-709 (1969).
- 33. Yang, X., Wang, Y., Yang, H. & Yang, Y. Experimental research on free settling properties of different types of single fiber particle in air. *Build. Environ.* **185**, 107300 (2020).
- Khayat, R. & Cox, R. Inertia effects on the motion of long slender bodies. J. Fluid Mech. 209, 435–462 (1989).
- Muñoz-Esparza, D., Sharman, R. D. & Lundquist, J. K. Turbulence dissipation rate in the atmospheric boundary layer: observations and WRF mesoscale modeling during the XPIA field campaign. *Mon. Weather Rev.* 146, 351–371 (2018).
- Batchelor, G. Slender-body theory for particles of arbitrary cross-section in Stokes flow. J. Fluid Mech. 44, 419–440 (1970).
- Ni, R., Kramel, S., Ouellette, N. T. & Voth, G. A. Measurements of the coupling between the tumbling of rods and the velocity gradient tensor in turbulence. J. Fluid Mech. 766, 202–225 (2015).

- 38. Clift, R., Grace, J. R. & Weber, M. E. Bubbles, Drops, and Particles (Dover Publications, 2005).
- Huang, Y., Adebiyi, A. A., Formenti, P. & Kok, J. F. Linking the different diameter types of aspherical desert dust indicatesthat models underestimate coarse dust emission. *Geophys. Res. Lett.* 48, e2020GL092054 (2021).
- Evangeliou, N. et al. Atmospheric transport is a major pathway of microplastics to remote regions. Nat. Commun. 11, 3381 (2020).
- Allen, S. et al. Examination of the ocean as a source for atmospheric microplastics. PloS ONE 15, 0232746 (2020).
- 42. Yang, S. et al. Constraining microplastic particle emission flux from the ocean. *Environ. Sci. Technol. Lett.* **9**, 513–519 (2022).
- 43. Oehmke, T. & Variano, E. A new particle for measuring mass transfer in turbulence. *Exp. Fluids* **62**, 16 (2021).
- 44. Cheng, K.-Y., Wang, P. K. & Hashino, T. A numerical study on the attitudes and aerodynamics of freely falling hexagonal ice plates. *J. Atmos. Sci.* **72**, 3685–3698 (2015).

Publisher's note Springer Nature remains neutral with regard to jurisdictional claims in published maps and institutional affiliations.

Springer Nature or its licensor (e.g. a society or other partner) holds exclusive rights to this article under a publishing agreement with the author(s) or other rightsholder(s); author self-archiving of the accepted manuscript version of this article is solely governed by the terms of such publishing agreement and applicable law.

© The Author(s), under exclusive licence to Springer Nature Limited 2023

Methods

Mean settling rate based on linearized slender-body theory

In this study, we seek a formulation of the mean settling rate for atmospheric MPFs by combining theoretical results from slender-body theory^{34,36} and recent results from numerical experiments^{28,29}. Such a combination leads to a physically based semi-analytical model for inertial MPFs settling in turbulent air, where the orientation statistics of fibres are incorporated into the model. A flowchart summarizing the current approach is presented in Extended Data Fig. 7. Here adopting a similar approach to ref. 21, we consider a linearized version of the slender-body theory model for elongated particles at finite particle Reynolds number Re₁ = $(w_{fi}w_{fi})^{\frac{1}{2}}l/v$, where *l* is the half length over its long axis, v is the kinematic viscosity of ambient fluid and w_{fi} is the terminal settling velocity³⁴. The settling velocity can be expressed using a standard mobility matrix formalism²¹ as a consequence of the balance among gravitational force, buoyancy force and aerodynamic forces. This approach avoids iteratively solving the nonlinear equations in the original model34 that is computationally costly45, making it feasible for application in atmospheric transport modelling. The average settling velocity of MPFs depends on fibres' orientation as will be shown later. It is impractical in global and regional atmospheric models to model the rotational dynamics of each fibre. Thus, a simplified approach involving the fibres' orientation statistics is proposed. The experimental results from refs. 28 and 29 provide a foundation in the current work to parameterize the orientation statistics by considering the relative effects of inertial and turbulent torques that modify the equilibrium orientation of a fibre with a given shape. This is especially important for many existing observations of deposited atmospheric MPFs, as many have lengths longer than 100 μ m and a finite Re₁ of O(10), which means that the fluid inertial torque acting on the fibre becomes important^{28,29,45}. In fact, the rotational dynamics of fibrous inertialess particles under shear Stokes flow is typically characterized through Jeffery's orbits^{46,47}, where the contribution of convective fluid inertia to the change of angular motions are negligible. Thus, the current approach can be seen as a correction to the inertialess rotation of the fibre with added fluid inertial torques.

For MPF with Re₁ up to O(10), $w_{\rm f,i}$ is achieved when the drag force and F_3 , the sum of gravitational and buoyancy forces, are in balance if no further external forces are considered. Here a regular Cartesian coordinate system is considered, and 3 represents the component in the vertical direction and similar definitions are given for the rest along the horizontal plane. This can mathematically be expressed as $w_{\rm f,i} = M_{\rm i3}F_3$, in which $M_{\rm i3}$ is the mobility matrix relating the forces to motion²¹. F_3 can be further denoted as $2lA_{\rm f}(\rho_{\rm f}-\rho_{\rm a})$ g, where $A_{\rm f}$ is the cross-sectional area of MPF, g is the gravitational constant, $\rho_{\rm f}$ is MPF density and $\rho_{\rm a}$ is the density of ambient fluid (in this case air). With simple operations, $w_{\rm f,i}$ can be formalized as follows:

$$w_{f,i} = 2M_{i3}lA_f(\rho_f - \rho_a)g.$$
 (1)

MPFs are assumed to have a constant density. A circular/elliptical cross-sectional shape $A_{\rm f}$ (Fig. 2a) is considered for simplicity. Informed by observations of deposited atmospheric MPFs^{4,5}, two types of fibre, namely 'round' and 'flat', will be represented by $A_{\rm f}$ being circular with diameter D and elliptical with semi-major axis b=D/2, semi-minor axis c. The diameter D of round fibre is also referred to as the width. The minimum dimension of a flat fibre 2c is referred to as the thickness. Note that existing measurements obtain the dimension 2b, where the determination of 2c can have large uncertainties. Following the assumption in ref. 4 about the minimum dimension of the cross sections being $2\,\mu\text{m}$, we consider the thickness of flat fibres to be $2\,\mu\text{m}$ ($c=1\,\mu\text{m}$) for subsequent analyses. In general, the mobility matrix M_{ij} reads²¹

$$M_{ij} = M_{\parallel} p_i p_j + M_{\perp} (\delta_{ij} - p_i p_j), \tag{2}$$

where δ_{ij} is the identity matrix, p_i is the orientation vector of the MPF and M_{\parallel} and M_{\perp} are the mobility coefficients for $\theta=0$ and $\theta=\pi/2$, respectively, where θ is the azimuthal angle between MPF orientation and vertical plane. The expressions of M_{\parallel} and M_{\perp} can be found in the Supplementary Information.

The instantaneous settling velocity $w_{\rm f,i}$ of MPF highly depends on its orientation vector p_i , which is justified by the well-known result that an elongated MPF will have a doubled settling velocity if θ changes from $\pi/2$ to 0 (refs. 21,27,34,36). Besides, the MPF falling in the atmosphere presents rich orientation dynamics due to the rotational torque exerted by the ambient turbulence²⁷. Therefore, to avoid tracking the complicated orientation evolution, a time-averaged MPF settling velocity is adopted if the observation time window length T_0 is long enough to allow the MPF to experience all possible orientations. For a typical round fibre with diameter $D \le 50 \, \mu \text{m}$ (refs. 4,17) and small $\text{Re}_D = (w_{\text{f,i}} w_{\text{f,i}})^{\frac{1}{2}} D / \nu \le 1$ (refs. 25,28,29), it has a fast tumbling rate approximately as 10 rad s⁻¹ (ref. 48) compared with the relatively slower settling velocity (up to O(0.1) m s⁻¹) (refs. 32,48). Additionally, the representative maximum tilt angle of MPFs with $D \ge 20 \,\mu\text{m}$ is ~ 0.1 rad (ref. 49). The orientation distribution of MPFs with $D \le 10 \mu m$ is easily randomized by turbulence with the characteristic settling velocity up to $\sim 0.01 \, \mathrm{m \, s^{-1}}$ (ref. 50). In practice, T_0 can be selected as short as 0.1~1s for the aforementioned two extreme cases with equivalent falling distance ~ 0.01 m, in which the MPF undergoes all possible orientations. These values of T_0 are much shorter than the time step of typical regional and global atmospheric transport models, thus considering time-averaged orientation is a justified approach here. The orientation of MPF is characterized by a $\theta - \phi$ joint probability density function $\Phi(\theta, \phi)$, where ϕ is the polar angle. A uniform ϕ distribution is expected owing to the cylindrical symmetry of the flow system⁵¹, which is a valid approximation for the scenario that the body forces acting upon the MPF is only along the vertical direction, and the background shear flow is practically negligible compared with turbulent strength (in the atmosphere far away from the ground where their velocity gradient magnitude ratio is typically less than 0.1; Supplementary Information for details). Additionally, due to the foreaft symmetry of the MPF, the $\Phi(\theta, \phi)$ can be further simplified as⁵¹

$$\int_0^{\pi/2} \Phi(\theta) \sin \theta d\theta = \frac{1}{4\pi}.$$
 (3)

Within T_0 , the time-averaged $w_{\rm f,3}$ is symbolized as $\overline{w}_{\rm f,3}$, which is equivalent to its orientation averaged counterpart due to the selection of T_0 . Similar operations are taken for $w_{\rm f,1}$ and $w_{\rm f,2}$ and they would vanish (Supplementary Information for details), leaving $\overline{w}_{\rm f,3}$ being the only non-zero component, which is denoted as $w_{\rm s}$ hereafter. By this time-averaged operation on equations (1) and (2), the formulation of $w_{\rm s}$ is derived as follows:

$$\begin{split} w_{\rm S} &= \overline{w}_{\rm f,3} = \left[M_{\perp} + \frac{(M_{\parallel} - M_{\perp})}{T_0} \int_0^{T_0} \cos^2 \theta(t) dt \right] 2l A_{\rm f}(\rho_{\rm f} - \rho_{\rm a}) \mathrm{g} \\ &= \left[M_{\perp} + (M_{\parallel} - M_{\perp}) \int_0^{\pi/2} \Phi(\theta) \cos^2 \theta \sin \theta d\theta \right] 2l A_{\rm f}(\rho_{\rm f} - \rho_{\rm a}) \mathrm{g} \\ &= \left[M_{\perp} + (M_{\parallel} - M_{\perp}) \langle \cos^2 \theta \rangle \right] 2l A_{\rm f}(\rho_{\rm f} - \rho_{\rm a}) \mathrm{g}, \end{split}$$

$$(4)$$

Here $\langle\cos^2\theta\rangle$ is the orientation variance of $\cos\theta$ and the equilibrium orientation is $\theta=\pi/2$ (refs. 28,29). In equation (4), M_{\parallel} and M_{\perp} are treated as approximately time independent because the convective inertial corrections are not leading-order terms when the orientation and thus settling velocity varies²¹.

Rotational dynamics of MPFs

The rotational dynamics of MPF are determined by the angular equations of motion, which includes the inertial torque $\frac{5\pi\rho_f\ell^5}{3(\ln^22\beta)}(\mathbf{w}_f\cdot\mathbf{p})(\mathbf{w}_f\times\mathbf{p})$

(ref. 34), rotational drag torque $\frac{8n\mu l^3}{3(\ln 2\beta)}$ ($\Omega_s \times \mathbf{p}$) (refs. 36,46) and torque from turbulent strain $\frac{8n\mu l^3}{3(\ln 2\beta)}$ ($\mathbf{p} \times (\mathbf{S} \cdot \mathbf{p})$) (refs. 28,29). Here \mathbf{w}_f represents

the settling velocity of the fibre, **p** denotes the fibre orientation, $\Omega_{\rm s}$ signifies rotation resulting from the slip velocity and **S** corresponds to the turbulent strain. For MPFs observed in the air, their diameters or widths are typically around 10-20 µm, resulting in corresponding Reynolds numbers Rep based on their settling velocity and diameters/ widths that are smaller than 0.5. This means that the particle inertia effect can be treated as negligible. On the contrary, the Reynolds numbers Re₁ based on the fibre length can indeed be up to O(10) and the fluid inertial torque cannot be neglected. This torque occurs due to the added mass effect and will be lower for flat fibres that have the same width as round fibres but settle more slowly. Consequently, it becomes critical for researchers to enumerate both Rep and Rel to identify the conditions under which the particle inertial effects in the inner region and fluid inertial torque can either be disregarded or must be taken into account.

The effect of torque from turbulent strain can be characterized by the turbulent time scale τ_{turb} . Similarly, the net contribution of MPF fluid inertial and rotational drag torques can be identified by the inverse of its zero-torque tumbling rate $\tau_{\text{sed},\theta=45^{\circ}}$ as defined by Kramel²⁸. Accordingly, the ratio between the two aforementioned time scales $S_F = \tau_{turb}/\tau_{sed,\theta=45^{\circ}}$ can be exploited to represent the relative strength between inertial and turbulent effects and thus determine the orientation statistics^{28,29}. The explicit expressions of the above parameters are given in Supplementary Information. When $S_E \ll 1$, the rotations due to turbulence are strong compared to rotations due to inertial torque, leading to the randomized motion of MPF and $\langle \cos^2 \theta \rangle = 1/3$. For $S_F \gg 1$, inertial torque dominates its rotational motion and the MPF falls with its major axis facing approximately horizontally. The detailed dependence of orientation variance $\langle \cos^2 \theta \rangle$ on S_F has been obtained experimentally in the intermediate range and theoretically in the two extreme cases as following^{28,29},

$$\langle \cos^2 \theta \rangle = \begin{cases} 1/3 & S_F \le 0.1 \\ 0.07531S_F^{-0.6692} - 0.0188 & 0.1 < S_F < 5.0 \\ \frac{2}{15S_F^2} & S_F \ge 5.0 \end{cases}$$
 (5)

The expression of orientation variance in the intermediate range shown above has been obtained by fitting experimental data in refs. 28,29 via a power law. Thus, a predictive model of the mean settling rate of MPF of a given size, shape and density immersed in turbulence is given by equations (4) and (5). In addition, consideration of S_F gives us some physical intuitions behind the difference between round and fibre rotational dynamics. For example, the round fibre is expected to have a smaller orientation variance compared with the flat fibre with given ambient turbulence. The rotational drag torque, which is a part of the Jeffery torque, is a result of the slip between fluid and particle, and less settling velocity indicates less slip and less rotational drag torque. Overall, round fibres generally experience higher inertial torque and rotational drag torque than flat fibres. The relative strength of these two torques can be quantified by the time scale of the zero-torque tumbling rate in quiescent

flow, which is approximated as $au_{\rm sed, \theta=45^{\circ}} \sim rac{8 {
m vin} eta}{w_{l, \rm min}^2}$. This demonstrates that

round fibres, which have a higher settling velocity, are more dominantly influenced by fluid inertia that reduces the impact of ambient turbulence, compared to flat fibres. In conclusion, flat fibres experience a higher relative value of turbulent torque compared to other torques, which results in a greater degree of randomization as shown in Fig. 2d.

Source estimation using the proposed new settling velocity model

A previous study has used a detailed dataset from the western United States, atmospheric modelling and an optimal estimation to estimate the sources of microplastics in the western United States, a large portion of which are MPFs⁴. The simulations occur for the same time period as the observations. The transport and deposition are simulated at the sites where the observations are made. An optimal estimation method is used to deduce the magnitude of each of the five sources that has the best match to the observations (forcing the sources to be non-negative) using a Chi-squared cost function approach. The estimated errors are modified to allow the cost function value to be approximately the number of observations. The 95% confidence limits are found from the Chi-squared values, allowing an estimate of the errors to be obtained. Using the new theory for each size fraction, we can estimate their deposition velocities. We convert these velocities to an equivalent diameter using the standard theory¹⁵ and use the existing model runs to show the importance of these changes. To emphasize the importance of differences between the round and flat fibres, we conduct two separate optimal estimations assuming that all fibres have round cross-sectional shapes or alternatively all fibres are flat.

Data availability

Original data underlying the figures are available at https://github. com/a20070348/MPFs_Data.

Code availability

Code for computing the settling velocity given different characteristics of the fibres is available at https://github.com/a20070348/MPs.

References

- 45. Roy, A., Hamati, R. J., Tierney, L., Koch, D. L. & Voth, G. A. Inertial torques and a symmetry breaking orientational transition in the sedimentation of slender fibres. J. Fluid Mech. 875, 576-596 (2019).
- 46. Jeffery, G. B. The motion of ellipsoidal particles immersed in a viscous fluid. Proc. R. Soc. Lond. A 102, 161-179 (1922).
- 47. Ravnik, J., Marchioli, C. & Soldati, A. Application limits of jeffery's theory for elongated particle torques in turbulence: a DNS assessment. Acta Mech. 229, 827-839 (2018).
- Sabban, L., Cohen, A. & van Hout, R. Temporally resolved measurements of heavy, rigid fibre translation and rotation in nearly homogeneous isotropic turbulence. J. Fluid Mech. 814, 42-68 (2017).
- 49. Bréon, F.-M. & Dubrulle, B. Horizontally oriented plates in clouds. J. Atmos. Sci. 61, 2888-2898 (2004).
- 50. Klett, J. D. Orientation model for particles in turbulence. J. Atmos. Sci. 52, 2276-2285 (1995).
- Siewert, C., Kunnen, R., Meinke, M. & Schröder, W. Orientation statistics and settling velocity of ellipsoids in decaying turbulence. Atmos. Res. 142, 45-56 (2014).

Acknowledgements

We thank D.L. Koch for insightful scientific discussions and comments concerning this work. Our thanks also extend to Y. Guo and S. Yin for assistance with the illustrative figures. Q.L. acknowledges support from the US National Science Foundation (NSF-CAREER-2143664, NSF-AGS-2028633, NSF-CBET-2028842) and computational resources from the National Center for Atmospheric Research (UCOR-0049). J.B. acknowledges support from the US National Science Foundation (NSF-MSB-1926559).

Author contributions

S.X. and Q.L. designed this research. Y.C. helped with the data preparation and documentation of data and code. J.B. generated the data from on-site measurements. N.M.M. carried out large-scale climate modelling. S.X., Q.L. and N.M.M. wrote the manuscript draft. S.X., Q.L., N.M.M., J.B. and Y.C. revised the manuscript.

Competing interests

The authors declare no competing interests.

Inclusion and ethics

All authors are committed to fostering an inclusive and ethical environment in all aspects of our work.

Additional information

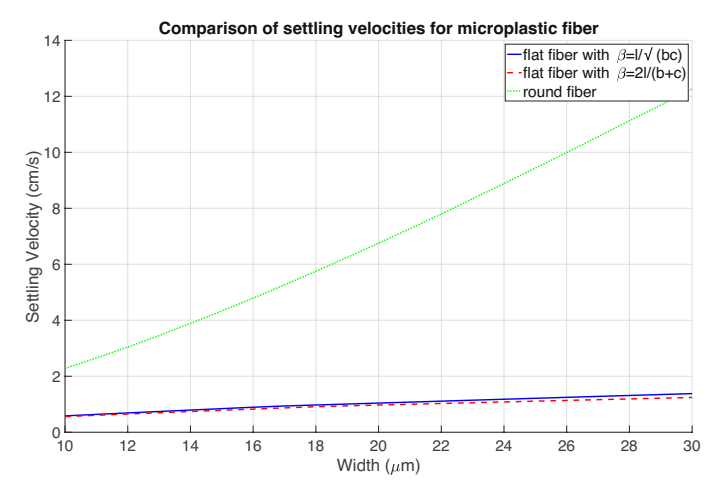
Extended data is available for this paper at https://doi.org/10.1038/s41561-023-01264-6.

Supplementary information The online version contains supplementary material available at https://doi.org/10.1038/s41561-023-01264-6.

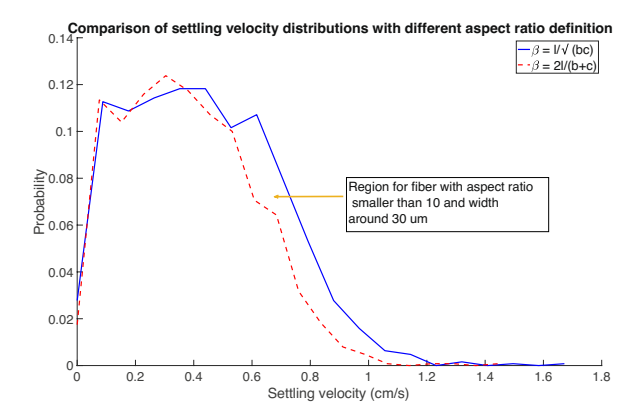
Correspondence and requests for materials should be addressed to Oi Li

Peer review information *Nature Geoscience* thanks Sajjad Abbasi, Cristian Marchioli, Masanori Saito, and the other, anonymous, reviewer(s) for their contribution to the peer review of this work. Primary Handling Editor: Xujia Jiang, in collaboration with the *Nature Geoscience* team.

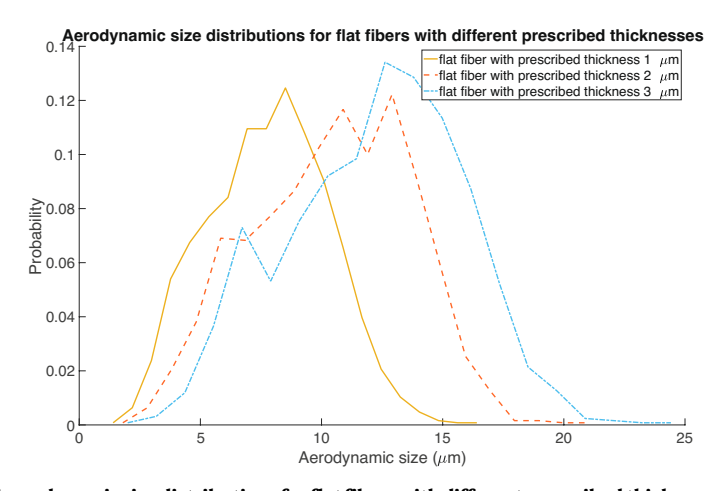
Reprints and permissions information is available at www.nature.com/reprints.



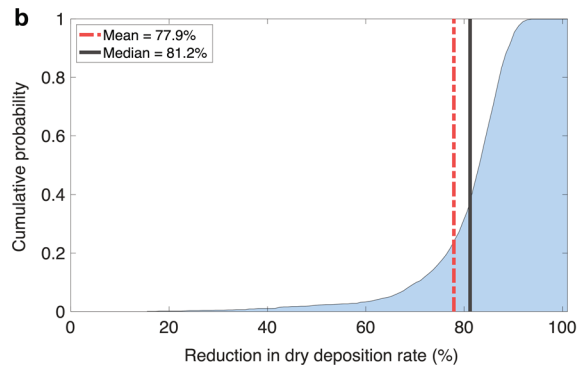
Extended Data Fig. 1 | Settling velocity for round fiber and flat fiber with $l=1\,mm$ and different β definition.

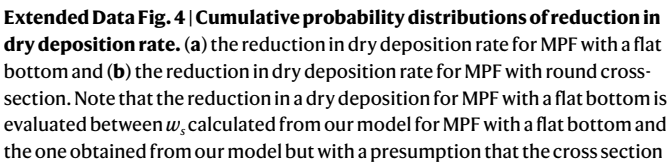


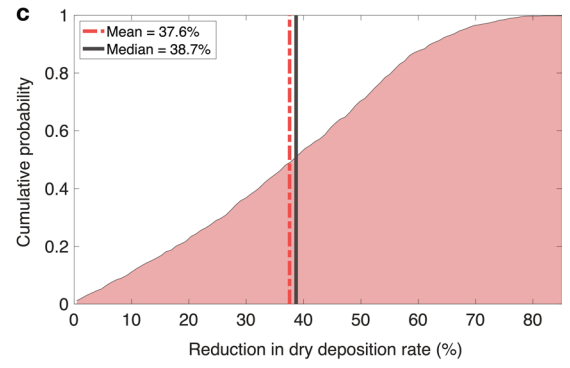
 $Extended\ Data\ Fig.\ 2\ |\ Settling\ velocity\ distribution\ for\ flat\ fiber\ with\ different\ \beta\ definition\ for\ field\ measurement\ data.$



 $Extended\ Data\ Fig.\ 3\ |\ Comparison\ of\ aerodynamic\ size\ distributions\ for\ flat\ fibers\ with\ different\ prescribed\ thicknesses.$

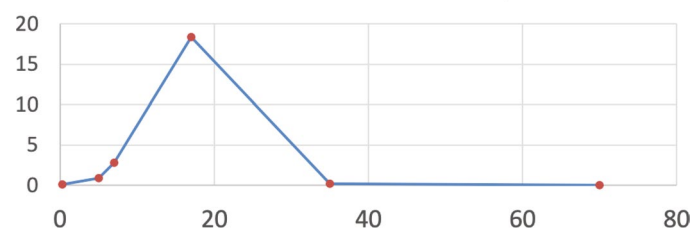






is in a round shape based on the sampled fiber on site. The reduction in dry deposition for MPF with a round cross section is compared between w_s calculated from our model and the one obtained from the volumetric spherical particle model. For all the subfigures, red dash–dot lines denote the mean quantities and black solid lines represent the median values.

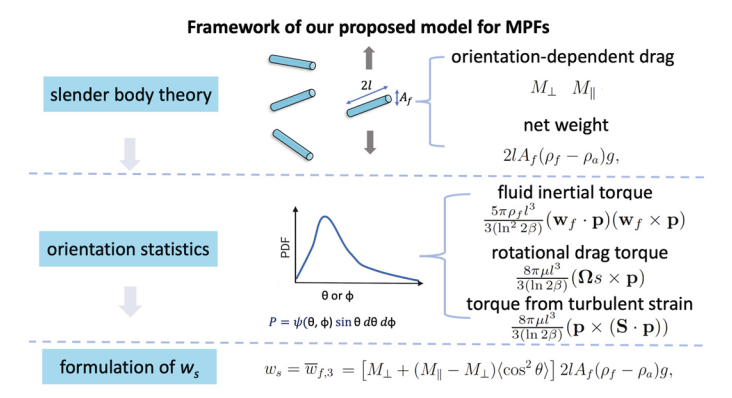
size of ocean source with size of plastics



 $Extended \ Data \ Fig. 5 \ | \ Figure \ showing \ the \ size \ of \ the \ ocean \ source \ (Tg \ on \ the \ y \ axis) \ as \ a \ function \ of \ the \ size \ of \ plastics \ (um \ on \ x-axis) \ in \ sensitivity \ studies \ where \ all \ plastics \ are \ assumed \ to \ be \ one \ size \ for \ each \ sensitivity \ study.$

Flowchart for implementing the proposed model for large-scale climate model width (2b) thickness (2c) density (ρ) Equation 16 in SI settling velocity w_S $D_{settling} = \sqrt{\frac{18\mu w_s}{(\rho_f - \rho_a)g}}$ aerodynamic size $D_{settling}$ Formulas/models widely used for dust particle transport and deposition Quantities related to MPFs transport and deposition such as travel distance, etc.

 $Extended \, Data \, Fig. \, 6 \, | \, Flow chart \, for \, implementing \, the \, proposed \, model \, for \, large-scale \, climate \, model.$



 $Extended\,Data\,Fig.\,7\,|\,Framework\,of\,our\,proposed\,settling\,velocity\,model\,for\,microplastic\,fiber.$